

# Lawrence Berkeley National Laboratory

## LBL Publications

### Title

Influence of LaFeO<sub>3</sub> Surface Termination on Water Reactivity

### Permalink

<https://escholarship.org/uc/item/1t9003q3>

### Journal

The Journal of Physical Chemistry Letters, 8(5)

### ISSN

1948-7185

### Authors

Stoerzinger, Kelsey A

Comes, Ryan

Spurgeon, Steven R

et al.

### Publication Date

2017-03-02

### DOI

10.1021/acs.jpcelett.7b00195

Peer reviewed

This document is confidential and is proprietary to the American Chemical Society and its authors. Do not copy or disclose without written permission. If you have received this item in error, notify the sender and delete all copies.

### Influence of LaFeO<sub>3</sub> Surface Termination on Water Reactivity

Journal:	<i>The Journal of Physical Chemistry Letters</i>
Manuscript ID	jz-2017-00195w.R1
Manuscript Type:	Letter
Date Submitted by the Author:	n/a
Complete List of Authors:	Stoerzinger, Kelsey; Pacific Northwest National Laboratory, Physical and Computational Sciences Directorate Comes, Ryan; Pacific Northwest National Laboratory, Physical and Computational Sciences Directorate; Auburn University, Physics Spurgeon, Steven; Pacific Northwest National Lab, Physical and Computational Sciences Directorate Thevuthasan, Suntharampillai; Pacific Northwest National Laboratory, Physical and Computational Sciences Directorate Ihm, Kyuwook; Pohang Accelerator Laboratory Crumlin, Ethan; E O Lawrence Berkeley National Laboratory, Advanced Light Source Chambers, Scott; Pacific Northwest National Laboratory, Physical and Computational Sciences Directorate

SCHOLARONE™  
Manuscripts

# Influence of LaFeO<sub>3</sub> Surface Termination on Water Reactivity

*Kelsey A. Stoerzinger,<sup>1,\*</sup> Ryan Comes,<sup>1,2</sup> Steven R. Spurgeon,<sup>1</sup> Suntharampillai Thevuthasan,<sup>1</sup>  
Kyuwook Ihm,<sup>3</sup> Ethan J. Crumlin,<sup>4</sup> Scott A. Chambers,<sup>1,\*</sup>*

<sup>1</sup>Physical and Computational Sciences Directorate, Pacific Northwest National Laboratory,  
Richland, Washington 99352, USA

<sup>2</sup>Department of Physics, Auburn University, Auburn, Alabama 36849, USA

<sup>3</sup>Pohang Accelerator Laboratory, Pohang, Kyungbuk, Korea

<sup>4</sup>Advanced Light Source, Lawrence Berkeley National Laboratory, Berkeley, California 94720,  
USA

## AUTHOR INFORMATION

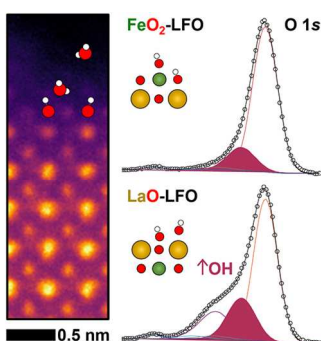
### Corresponding Author

\*kelsey.stoerzinger@pnnl.gov; sa.chambers@pnnl.gov

ABSTRACT The polarity of oxide surfaces can dramatically impact their surface reactivity, in particular with polar molecules such as water. The surface species that result from this interaction change the oxide electronic structure and chemical reactivity in applications such as

photoelectrochemistry, but are challenging to probe experimentally. Here we report a detailed study of the surface chemistry and electronic structure of the perovskite  $\text{LaFeO}_3$  in humid conditions using ambient pressure X-ray photoelectron spectroscopy. Comparing the two possible terminations of the polar (001)-oriented surface, we find that the LaO-terminated surface is more reactive toward water, forming hydroxyl species and adsorbing molecular water at lower relative humidity than its  $\text{FeO}_2$ -terminated counterpart. However, the  $\text{FeO}_2$ -terminated surface forms more hydroxyl species during water adsorption at higher humidity, suggesting adsorbate-adsorbate interactions may impact reactivity. Our results demonstrate how the termination of a complex oxide can dramatically impact its reactivity, providing insight that can aid in the design of catalyst materials.

## TOC GRAPHICS



Perovskite oxides such as  $\text{LaFeO}_3$  show great promise as catalysts for energy conversion and storage. Applications such as electrocatalysis,<sup>1-4</sup> photoelectrochemistry,<sup>5-7</sup> and gas sensing<sup>8-10</sup> all take place in an aqueous or humid environment, where the interaction with water plays a key role in determining the functionality of these complex oxides.<sup>11-13</sup> The formation of surface hydroxyl groups and adsorption of water can impact the surface electronic structure<sup>14</sup> and ultimately the mechanisms and kinetics of surface chemical reactions.<sup>15,16</sup> Initial studies have considered the reactivity of perovskites with water using ambient pressure X-ray photoelectron spectroscopy

1  
2  
3 (AP-XPS),<sup>12,17</sup> enabling study of the surface species present in equilibrium with water vapor. The  
4  
5 hydroxylation of these surfaces appeared greater than that of binary transition metal oxides.<sup>18</sup>  
6  
7  
8 However, the chemical nature of the hydroxyl site in such systems remained elusive due to the  
9  
10 unknown surface termination.

11  
12 The polar layers of (001)-oriented polar perovskite LaFeO<sub>3</sub> (LFO) have been the subject of  
13  
14 numerous recent investigations that consider the dipole formed at the (Nb-doped) SrTiO<sub>3</sub>  
15  
16 substrate-film interface<sup>19-21</sup> and the formation of a 2D metal at this interface<sup>22</sup>. However, despite  
17  
18 the promising photoelectrochemical activity<sup>5</sup> and sensing capabilities,<sup>9,10</sup> missing is an  
19  
20 experimental understanding of the surface properties for each layer. Density functional theory  
21  
22 (DFT) calculations report a lower work function for LaO- versus FeO<sub>2</sub>-termination,<sup>23</sup> which is  
23  
24 expected to result in notably different chemical reactivity. Of further interest is how the  
25  
26 electronic structure of each surface changes as a result of the formation of e.g. hydroxyl species,  
27  
28 where surface band bending in aqueous environments<sup>24</sup> is the critical component to charge  
29  
30 separation at the semiconductor/water interface in photoelectrochemical water splitting.  
31  
32  
33  
34  
35

36  
37 In the present work, we consider (001)-oriented epitaxial films of LFO distinctly terminated on  
38  
39 (LaO)<sup>+</sup> or (FeO<sub>2</sub>)<sup>-</sup> planes to probe the influence of perovskite surface termination on chemical  
40  
41 reactivity using ambient pressure X-ray photoelectron spectroscopy (AP-XPS).<sup>18,25,26</sup> We find  
42  
43 LaO-terminated LFO (LaO-LFO) is more reactive toward water, forming hydroxyl species at  
44  
45 lower relative humidities than its FeO<sub>2</sub>-terminated (FeO<sub>2</sub>-LFO) counterpart, consistent with DFT  
46  
47 calculations that indicate a greater stability of hydroxylated LaO-LFO.<sup>12</sup> The LaO surface is also  
48  
49 characterized by an additional surface oxygen species in both dry and humid conditions, the  
50  
51 formation of which is attributed to the positive charge of a (LaO)<sup>+</sup> layer and its high surface  
52  
53 energy. Core level shifts and changes in the gas-phase water peak indicate a downward band  
54  
55  
56  
57  
58  
59  
60

bending/flattening<sup>27</sup> and a decrease in work function,<sup>28</sup> respectively, resulting from hydroxylation and water adsorption.

Epitaxial 9 unit cell (u.c.) LFO films were fabricated by oxygen-assisted molecular beam epitaxy (MBE) on Nb-doped SrTiO<sub>3</sub> (001) surfaces at Pacific Northwest National Laboratory (Figure S1). The substrate was prepared with SrO or TiO<sub>2</sub> termination, resulting in LaO-LFO or FeO<sub>2</sub>-LFO, respectively (Figure 1). Cross-sectional high-angle annular dark field (STEM-HAADF) images, shown in Figure 1, confirm the excellent quality and epitaxy of the film. We observe differences in the surface termination, although damage resulting from TEM sample preparation makes it difficult to unambiguously identify the surface layer. Instead, the termination of the as-prepared film was confirmed by angle resolved XPS (Table S1) and remained unchanged during AP-XPS experiments (Figure S2).

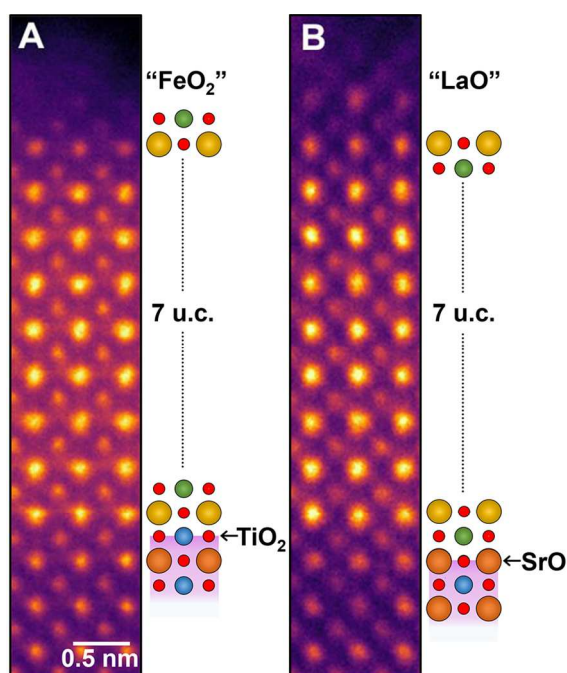


**Figure 1.** Colorized cross-sectional STEM-HAADF images and schematics of the 9 unit cell (u.c.) LaFeO<sub>3</sub>/Nb:SrTiO<sub>3</sub> films fabricated by oxygen assisted MBE. FeO<sub>2</sub>-LFO was grown on a

1  
2  
3 TiO<sub>2</sub>-terminated substrate (A), and LaO-LFO was grown on a SrO-terminated one (B). Surface  
4  
5 terminations were confirmed by angle resolved XPS (Table S1).<sup>19</sup>  
6  
7

8  
9 Upon introduction to the AP-XPS chamber at the Advanced Light Source, the films were  
10  
11 cleaned of ambient carbon contaminants by heating to 300 °C in 100 mTorr oxygen. The  
12  
13 resulting O 1s spectra are compared in Figure 2 (top panel) for the LaO- and FeO<sub>2</sub>-terminated  
14  
15 surface, with the C 1s spectra shown in the inset. For the FeO<sub>2</sub>-LFO, one main O 1s peak is  
16  
17 present, characteristic of bulk lattice oxygen, with a small shoulder at ~1.1 eV higher binding  
18  
19 energy attributed to hydroxyl (OH) species, the location of which was determined from  
20  
21 difference spectra during subsequent water dosing (Figure S3). For LaO-LFO, a third peak is  
22  
23 present at ~2.3 eV higher binding energy, termed “surf”. Such a surface feature has been often  
24  
25 observed for epitaxial perovskite films of unknown termination, as well as perovskite particles,  
26  
27 and has been attributed to a host of potential species such as carbonates,<sup>29,30</sup> adsorbed water,<sup>31,32</sup>  
28  
29 hydroxyls,<sup>31–33</sup> peroxide species,<sup>34</sup> undercoordinated oxygen,<sup>35,36</sup> and the terminal layer(s) of a  
30  
31 polar surface due to a shift in Madelung potential.<sup>17</sup> Considering the AP-XPS spectra collected at  
32  
33 300 °C in 100 mTorr oxygen (and similarly at ~24 mTorr oxygen, Figure S4), we rule out the  
34  
35 presence of carbonates and adsorbed water, and the lack of such a feature on the FeO<sub>2</sub>-terminated  
36  
37 surface suggests it does not arise from a change in Madelung potential at the surface. Instead, we  
38  
39 propose that the feature at ~2.3 eV above bulk oxygen arises from oxygen species present on the  
40  
41 surface with reduced screening, where DFT calculations on MgO surfaces support such a binding  
42  
43 energy offset for peroxo groups,<sup>34</sup> although a similar offset is also reported for OH groups on  
44  
45 MgO.<sup>37</sup> The higher surface energy of the LaO- versus FeO<sub>2</sub>-terminated surface predicted by  
46  
47 DFT<sup>12</sup> supports the model that the (LaO)<sup>+</sup> surface reconstructs chemically (adsorbing additional  
48  
49 oxygen) and/or electronically to compensate its polarity, while the (FeO<sub>2</sub>)<sup>-</sup> surface seems stable  
50  
51  
52  
53  
54  
55  
56  
57  
58  
59  
60

1  
2  
3 with only formation of a few hydroxyl groups (Figure 2B). A similar feature is observed on the  
4  
5 SrO-terminated surface of (001)-oriented SrTiO<sub>3</sub>, but not for the TiO<sub>2</sub> termination (Figure S5).  
6  
7

8 We next perform a water isobar to probe the LFO surfaces under different relative  
9  
10 humidity (RH). After removing oxygen gas, 100 mTorr H<sub>2</sub>O is introduced into the chamber at  
11  
12 300 °C (corresponding to a RH of 10<sup>-4</sup>%). The OH feature on LaO-LFO increases notably, while  
13  
14 that on FeO<sub>2</sub>-LFO increases only slightly (Figure 2 middle panel). The feature at ~2.3 eV on  
15  
16 LaO-LFO from undercoordinated oxygen/peroxo species persists in humid environments, which  
17  
18 might protonate with minimal shift in binding energy. A peak from gas phase water is present at  
19  
20 >5 eV higher binding energy than bulk oxygen. Further cooling leads to the formation of  
21  
22 adsorbed water (H<sub>2</sub>O<sub>ads</sub>) at ~3.4 eV above bulk oxygen (Figure 2 bottom panel), the location of  
23  
24 which is confirmed by difference spectra upon removal of water (Figure S6). The wider bulk  
25  
26 peak at higher temperatures is consistent with thermal (vibrational) broadening. Due to the high  
27  
28 propensity of LFO to form carbonate upon interaction with any residual CO<sub>2</sub> in the chamber,<sup>38</sup>  
29  
30 care was taken to quantify such species in the O 1s spectra from the intensity in the C 1s core  
31  
32 level (Experimental methods). All spectra were fit with the species described above with fitting  
33  
34 parameters found in Table S2, and depth profiling by changing the incident photon energy  
35  
36 confirms that the “surf” peak, OH, CO<sub>3</sub>, and H<sub>2</sub>O<sub>ads</sub> are located above that of the bulk (Figure  
37  
38  
39  
40  
41  
42  
43  
44  
45  
46  
47  
48  
49  
50  
51  
52  
53  
54  
55  
56  
57  
58  
59  
60 S7).



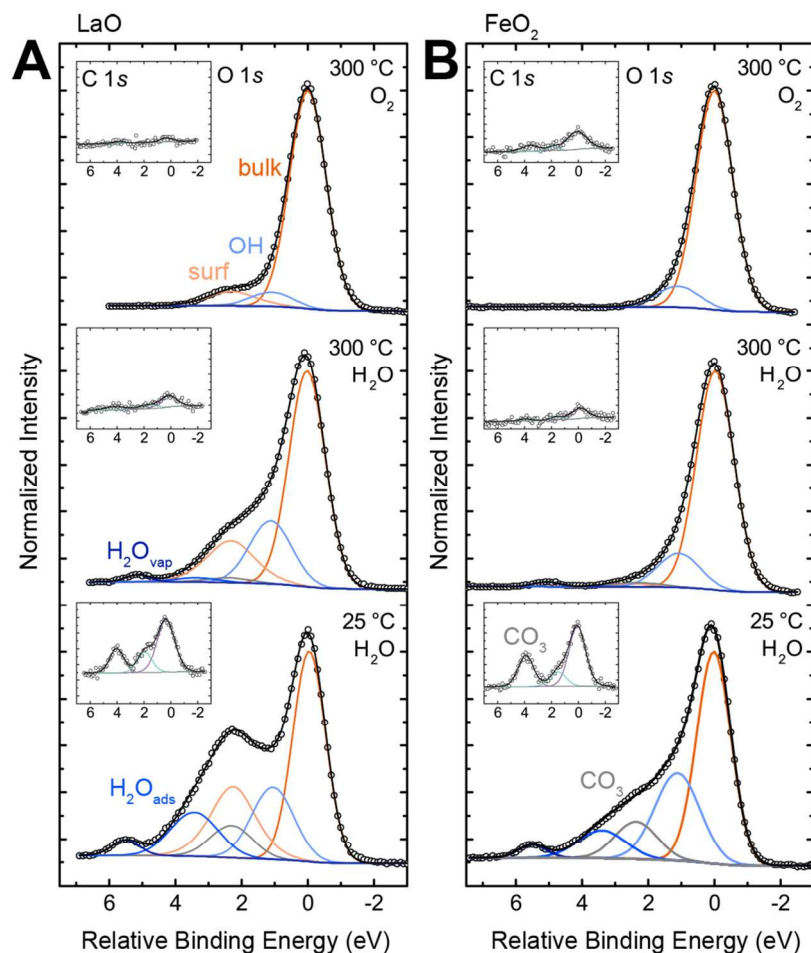


**Figure 2.** O 1s spectra and C 1s spectra (inset) for (A) LaO-LFO and (B) FeO<sub>2</sub>-LFO at 300 °C in 100 mTorr O<sub>2</sub> (top), 300 °C in 100 mTorr H<sub>2</sub>O (middle) and 25 °C in 100 mTorr H<sub>2</sub>O (bottom). Raw data are shown as points with fitted components and envelope (black) as lines. O 1s components correspond to the bulk oxide (orange), hydroxide (light blue), carbonate (gray), surface (peach), adsorbed water (medium blue), and gas phase water (dark blue). C 1s components correspond to carbonate (gray), adventitious carbon (purple), and an intermediate carbon oxidation (teal). The binding energy scale is shown relative to the bulk oxide (O 1s) and adventitious carbon (C 1s) to better illustrate relative offsets of species in fitting.

1  
2  
3 The chemical reactivity of each surface toward water can be assessed by considering the extent  
4 of hydroxyl species present as a function of RH. Figure 3A compares the OH and H<sub>2</sub>O<sub>ads</sub>  
5 components normalized to the bulk oxygen signal (likely canceling out any thermal broadening  
6 effects), with similar trends observed when considering them as a percentage of total oxygen  
7 signal (Figure S8) or using a multilayer electron attenuation model<sup>17</sup> to compute coverage  
8 (Figure S9, Table S3). Both terminations display similar OH contents in dry conditions (300 °C  
9 in 100 mTorr oxygen, yellow band in Figure 3A). In humid conditions, however, LaO-LFO is  
10 much more reactive toward water, with notable hydroxyl content at low RH. This is consistent  
11 with DFT calculations that report greater stability of hydroxylated LaO- versus FeO<sub>2</sub>-LFO.<sup>12</sup> The  
12 amount of hydroxyls on the LaO surface remains roughly constant upon further increase of RH  
13 during the isobar, suggesting sites with a high binding strength for hydroxyls saturate at low RH.  
14  
15  
16  
17  
18  
19  
20  
21  
22  
23  
24  
25  
26  
27  
28

29 The FeO<sub>2</sub>-terminated surface has notably less hydroxyl species at low RH, which remains  
30 constant until ~10<sup>-3</sup>% RH. At this point, H<sub>2</sub>O<sub>ads</sub> begins to form on the surface, and the amount of  
31 OH on FeO<sub>2</sub>-LFO increases in parallel. This is in direct contrast to the hydroxyl behavior of  
32 LaO-LFO, but similar to that observed on Fe<sub>3</sub>O<sub>4</sub><sup>39</sup> and Fe<sub>2</sub>O<sub>3</sub><sup>40</sup> surfaces, where it was attributed  
33 to adsorbate-adsorbate interactions. In contrast, LaO-LFO adsorbs more water at a given RH  
34 with a lower onset RH; however, this does not significantly impact the formation of OH species.  
35  
36  
37  
38  
39  
40  
41  
42  
43  
44  
45  
46  
47  
48  
49  
50  
51  
52  
53  
54  
55  
56  
57  
58  
59  
60

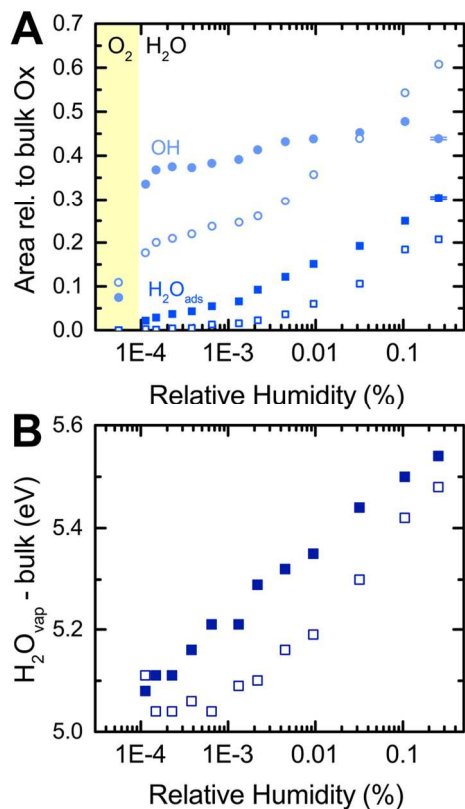


**Figure 3.** (A) Area of the OH (light blue, circles) and H<sub>2</sub>O<sub>ads</sub> (medium blue, squares) normalized to that of the bulk oxide as a function of RH probed by changing temperature in a 100 mTorr H<sub>2</sub>O isobar. Dry conditions (300 °C in 100 mTorr O<sub>2</sub>) are indicated with a yellow bar. LaO-LFO (solid) is more reactive toward water compared to FeO<sub>2</sub>-LFO (open). (B) Location of the gas-phase H<sub>2</sub>O<sub>vap</sub> peak relative to the bulk oxygen peak for LaO-LFO (solid) and FeO<sub>2</sub>-LFO (open) as a function of RH. The increase in binding energy corresponds to a decrease in sample work function, or formation of a surface dipole aiding photoelectron removal.

The use of AP-XPS also enables assessment of changes in the work function or surface dipole through shifts in the gas phase peak.<sup>28,41</sup> The H<sub>2</sub>O<sub>gas</sub> peak shifts to higher binding energy with RH, indicating a decrease in sample work function and/or formation of a surface dipole (Figure

1  
2  
3 3B). For example, adsorption of polar  $\text{OH}^-$  species have been shown to increase the surface  
4 potential of ceria.<sup>41</sup> This  $\sim 0.5$  eV shift is similar to that observed on  $\text{Fe}_3\text{O}_4$ ,<sup>39</sup> where DFT  
5 indicated adsorption of OH,  $\text{H}_2\text{O}$ , or co-adsorption of the two would lower the surface work  
6 function. For LFO, we highlight that the LaO-terminated surface exhibits a steady increase in gas  
7 phase binding energy with RH, while that of the  $\text{FeO}_2$ -terminated surface remains constant until  
8  $\sim 10^{-3}\%$  RH. This suggests that the decrease in work function is most influenced by the  
9 adsorption of polar water molecules, confirmed by its reversal upon decreasing the water  
10 pressure and desorbing  $\text{H}_2\text{O}_{\text{ads}}$  (Figure S10).  
11  
12  
13  
14  
15  
16  
17  
18  
19  
20  
21

22 Further insight regarding changes in the electronic structure upon OH and  $\text{H}_2\text{O}$  adsorption can  
23 be obtained from the metal core levels and valence band. Aside from changes to the lanthanum-  
24 oxygen ionicity reflected in the satellite intensity (Figure S11),<sup>42</sup> the line shape of the La 4d and  
25 Fe 3p are negligibly affected by the formation of OH and  $\text{H}_2\text{O}_{\text{ads}}$  groups. However, their absolute  
26 binding energies (Figure 4) are affected, with shifts to a higher binding energy reflecting  
27 downward band bending. This shift is greatest for LaO-LFO, which also exhibits greater  
28 reactivity toward water. The change in spectral intensity at  $\sim 2.5$  eV in  $\text{FeO}_2$ -LFO is not fully  
29 understood and merits further study.  
30  
31  
32  
33  
34  
35  
36  
37  
38  
39  
40  
41  
42  
43  
44  
45  
46  
47  
48  
49  
50  
51  
52  
53  
54  
55  
56  
57  
58  
59  
60

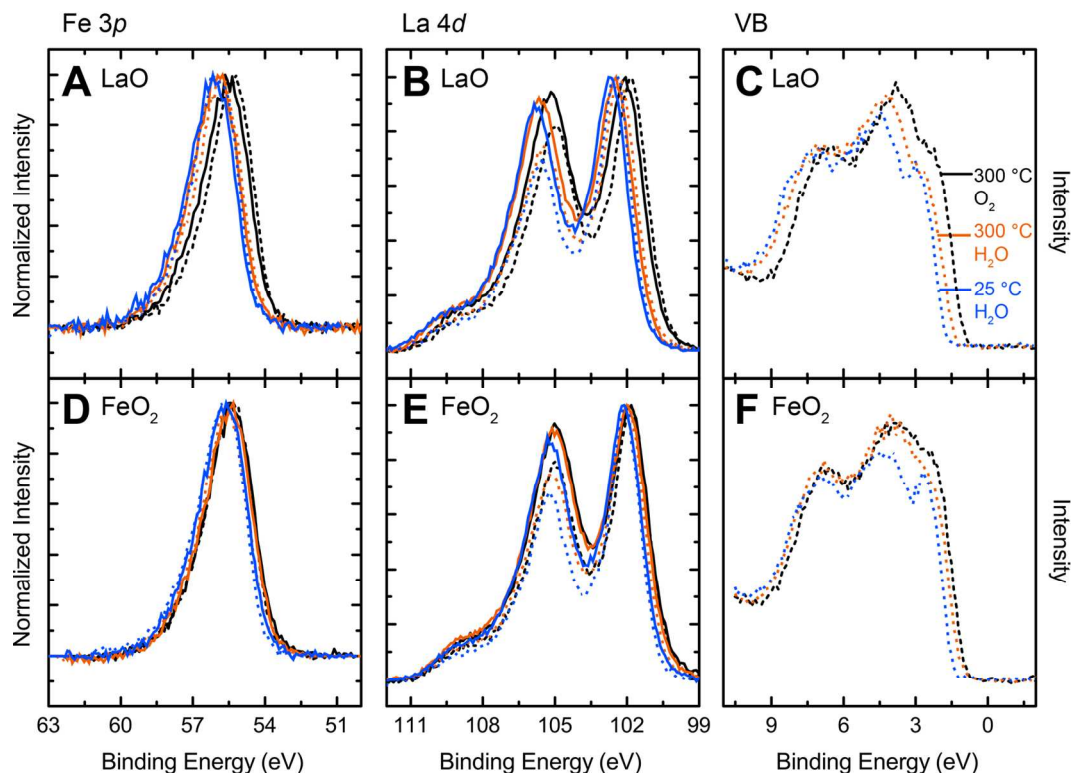


**Figure 4.** Noted Fe 3p, La 4d core levels and valence band (VB) for (A-C) LaO-LFO and (D-F) FeO<sub>2</sub>-LFO. Solid lines are for 690 eV incident photon energy with a larger information depth than dashed lines for 350 eV. Conditions are 300 °C in 100 mTorr O<sub>2</sub> (black), 300 °C in 100 mTorr H<sub>2</sub>O (orange) and 25 °C in 100 mTorr H<sub>2</sub>O (blue). The shift to higher binding energies with increasing RH corresponds to downward band bending, and is greater for LaO-LFO.

In conclusion, we have presented a detailed study of the interaction between water and (001)-oriented LaFeO<sub>3</sub> films terminated with either the LaO or FeO<sub>2</sub> plane. Using ambient pressure X-ray photoelectron spectroscopy to probe the surface species present in equilibrium with gas phase water, we find greater hydroxylation of the LaO- versus FeO<sub>2</sub>-LFO surface at low humidity, consistent with previous reports using DFT. However, the ultimately larger amount of OH on FeO<sub>2</sub>-LFO at high humidity (commensurate with water adsorption) suggests adsorbate-

1  
2  
3 adsorbate interactions may play an important role in dictating reactivity. An additional surface  
4 oxygen species often observed on perovskites is present only on the LaO termination, such as a  
5 peroxy group that could protonate in humid conditions. Core level shifts and changes in the gas-  
6 phase water peak indicate a downward band bending/flattening and a decrease in work function,  
7 respectively, upon interaction with water. This experimental study of the impact of termination  
8 in complex oxides on chemical reactivity and the resultant electronic structure brings new insight  
9 to applications such as photoelectrocatalysis.  
10  
11  
12  
13  
14  
15  
16  
17  
18  
19  
20  
21

## 22 **Experimental Methods**

23  
24 *Film growth* LFO/*n*-STO(001) heterojunctions were prepared using oxygen-assisted MBE.  
25 Films were grown at  $600 \pm 50^\circ\text{C}$  at a rate of one monolayer (either LaO or FeO<sub>2</sub>) every 43  
26 seconds using effusion cells and alternately shuttering the La and Fe beams, with a mixed O/O<sub>2</sub>  
27 beam generated by an electron cyclotron resonance source continuously incident on the  
28 substrate.<sup>43</sup> A pair of 0.05% Nb-doped STO substrates (Crystec) were prepared side-by-side  
29 using a boiling deionized water treatment,<sup>44</sup> followed by an anneal in air at 1000 °C for 30  
30 minutes. The samples were then cleaned in ozone on the bench and loaded into an oxide MBE  
31 system (DCA) with an appended x-ray photoelectron spectrometer (VG Scienta R3000 analyzer  
32 and monochromatic Al K $\alpha$  x-ray source). The TiO<sub>2</sub> termination was confirmed using angle-  
33 resolved XPS measurements (Table S1). A single monolayer of SrO was then deposited using an  
34 effusion cell on one of the substrates to achieve the A-site termination, also confirmed by angle-  
35 resolved XPS.<sup>19</sup> Increments of three u.c. (1 u.c. =  $\sim 3.9\text{\AA}$ ) of LFO were then grown with a  
36 shuttering sequence configured to match the substrate termination (i.e. FeO<sub>2</sub> (LaO) layer  
37 deposited first on the SrO- (TiO<sub>2</sub>-) terminated substrate) up to a total of 9 u.c.  
38  
39  
40  
41  
42  
43  
44  
45  
46  
47  
48  
49  
50  
51  
52  
53  
54  
55  
56  
57  
58  
59  
60

1  
2  
3 *Ambient pressure X-ray photoelectron Spectroscopy* AP-XPS was collected at Beamline 9.3.2  
4 at Lawrence Berkeley National Laboratory's (LBNL) Advanced Light Source (ALS).<sup>45</sup> LFO  
5 films were placed directly onto a ceramic heater and held in place by spring-loaded Inconel tips  
6 separated with an Al<sub>2</sub>O<sub>3</sub> spacer. The film was grounded through a thermocouple pressed into a  
7 gold foil placed directly onto the sample surface for temperature measurements and isolated from  
8 the sample holder clip with an Al<sub>2</sub>O<sub>3</sub> spacer. Further fitting details are provided in the  
9 Supplemental Information.  
10  
11  
12  
13  
14  
15  
16  
17  
18  
19  
20  
21

## 22 ASSOCIATED CONTENT

23  
24  
25 **Supporting Information.** Additional spectra, further spectral analysis, XPS fitting procedure,  
26 and TEM methods are available free of charge via the Internet at <http://pubs.acs.org>.  
27  
28  
29  
30

## 31 AUTHOR INFORMATION

### 32 Notes

33  
34  
35 The authors declare no competing financial interests.  
36  
37  
38

## 39 ACKNOWLEDGMENT

40  
41  
42 APXPS measurements and analysis were supported for K.A.S. by the Linus Pauling  
43 Distinguished Post-doctoral Fellowship at Pacific Northwest National Laboratory (PNNL LDRD  
44 69319), and for S.T. by the chemical imaging initiative, an LDRD program at PNNL. Film  
45 growth and characterization was supported at PNNL by the U.S. Department of Energy, Office  
46 of Science, Division of Materials Sciences and Engineering under Award No. 10122. The PNNL  
47 work was performed in the Environmental Molecular Sciences Laboratory (EMSL), a national  
48 science user facility sponsored by the Department of Energy's Office of Biological and  
49  
50  
51  
52  
53  
54  
55  
56  
57  
58  
59  
60

1  
2  
3 Environmental Research and located at Pacific Northwest National Laboratory. The ALS is  
4 supported by the Director, Office of Science, Office of Basic Energy Sciences of the US DOE at  
5  
6 the Lawrence Berkeley National Laboratory under Contract DE-AC02-05CH11231.  
7  
8  
9

10  
11 REFERENCES  
12

- 13  
14 (1) Suntivich, J.; May, K. J.; Gasteiger, H. A.; Goodenough, J. B.; Shao-Horn, Y. A  
15 Perovskite Oxide Optimized for Oxygen Evolution Catalysis from Molecular Orbital  
16 Principles. *Science*. **2011**, *334*, 1383–1385.  
17  
18  
19 (2) Suntivich, J.; Gasteiger, H. A.; Yabuuchi, N.; Nakanishi, H.; Goodenough, J. B.; Shao-  
20 Horn, Y. Design Principles for Oxygen-Reduction Activity on Perovskite Oxide Catalysts  
21 for Fuel Cells and Metal-Air Batteries. *Nat. Chem.* **2011**, *3*, 546–550.  
22  
23  
24 (3) Man, I. C.; Su, H. Y.; Calle-Vallejo, F.; Hansen, H. A.; Martínez, J. I.; Inoglu, N. G.;  
25 Kitchin, J.; Jaramillo, T. F.; Nørskov, J. K.; Rossmeisl, J. Universality in Oxygen  
26 Evolution Electrocatalysis on Oxide Surfaces. *ChemCatChem* **2011**, *3*, 1159–1165.  
27  
28  
29 (4) Jacobson, A. J. Materials for Solid Oxide Fuel Cells. *Chem. Mater.* **2010**, *22*, 660–674.  
30  
31  
32 (5) May, K. J.; Fenning, D. P.; Ming, T.; Hong, W. T.; Lee, D.; Stoerzinger, K. A.; Biegalski,  
33 M. D.; Kolpak, A. M.; Shao-Horn, Y. Thickness-Dependent Photoelectrochemical Water  
34 Splitting on Ultrathin LaFeO<sub>3</sub> Films Grown on Nb:SrTiO<sub>3</sub>. *J. Phys. Chem. Lett.* **2015**, *6*,  
35 977–985.  
36  
37  
38 (6) Peng, Q.; Wang, J.; Wen, Y. W.; Shan, B.; Chen, R. Surface Modification of LaFeO<sub>3</sub> by  
39 Co-Pi Electrochemical Deposition as an Efficient Photoanode under Visible Light. *RSC*  
40 *Adv.* **2016**, *6*, 26192–26198.  
41  
42  
43  
44  
45  
46  
47  
48  
49  
50  
51  
52  
53  
54  
55  
56  
57  
58  
59  
60



- 1  
2  
3 (7) Parida, K. M.; Reddy, K. H.; Martha, S.; Das, D. P.; Biswal, N. Fabrication of  
4 Nanocrystalline LaFeO<sub>3</sub>: An Efficient Sol-Gel Auto-Combustion Assisted Visible Light  
5 Responsive Photocatalyst for Water Decomposition. *Int. J. Hydrogen Energy* **2010**, *35*,  
6 12161–12168.  
7  
8  
9  
10  
11  
12 (8) Fergus, J. W. Perovskite Oxides for Semiconductor-Based Gas Sensors. *Sensors*  
13 *Actuators, B Chem.* **2007**, *123*, 1169–1179.  
14  
15  
16  
17  
18 (9) Toan, N. N.; Saukko, S.; Lantto, V. Gas Sensing with Semiconducting Perovskite Oxide  
19 LaFeO<sub>3</sub>. *Phys. B Condens. Matter* **2003**, *327*, 279–282.  
20  
21  
22  
23  
24 (10) Zhao, J.; Liu, Y.; Li, X.; Lu, G.; You, L.; Liang, X.; Liu, F.; Zhang, T.; Du, Y. Highly  
25 Sensitive Humidity Sensor Based on High Surface Area Mesoporous LaFeO<sub>3</sub> Prepared by  
26 a Nanocasting Route. *Sensors Actuators, B Chem.* **2013**, *181*, 802–809.  
27  
28  
29  
30  
31  
32 (11) Nenning, A.; Navickas, E.; Hutter, H.; Fleig, J. Water-Induced Decoupling of Tracer and  
33 Electrochemical Oxygen Exchange Kinetics on Mixed Conducting Electrodes. *J. Phys.*  
34 *Chem. Lett.* **2016**, *7*, 2826–2831.  
35  
36  
37  
38  
39 (12) Stoerzinger, K. A.; Hong, W. T.; Azimi, G.; Giordano, L.; Lee, Y. L.; Crumlin, E. J.;  
40 Biegalski, M. D.; Bluhm, H.; Varanasi, K. K.; Shao-Horn, Y. Reactivity of Perovskites  
41 with Water: Role of Hydroxylation in Wetting and Implications for Oxygen  
42 Electrocatalysis. *J. Phys. Chem. C* **2015**, *119*, 18504–18512.  
43  
44  
45  
46  
47  
48 (13) Rubasinghege, G.; Elzey, S.; Baltrusaitis, J.; Jayaweera, P. M.; Grassian, V. H. Reactions  
49 on Atmospheric Dust Particles: Surface Photochemistry and Size-Dependent Nanoscale  
50 Redox Chemistry. *J. Phys. Chem. Lett.* **2010**, *1*, 1729–1737.  
51  
52  
53  
54  
55  
56  
57  
58  
59  
60

- 1  
2  
3  
4  
5  
6  
7  
8  
9  
10  
11  
12  
13  
14  
15  
16  
17  
18  
19  
20  
21  
22  
23  
24  
25  
26  
27  
28  
29  
30  
31  
32  
33  
34  
35  
36  
37  
38  
39  
40  
41  
42  
43  
44  
45  
46  
47  
48  
49  
50  
51  
52  
53  
54  
55  
56  
57  
58  
59  
60
- (14) Henderson, M. A. The Interaction of Water With Solid Surfaces : Fundamental Aspects. *Surf. Sci. Rep.* **2002**, *46*, 1–308.
- (15) Brown Jr., G. E.; Henrich, V. E.; Casey, W. H.; Clark, D. L.; Eggleston, C.; Felmy, A.; Goodman, D. W.; Graetzel, M.; Maciel, G.; McCarthy, M. I.; et al. Metal Oxide Surfaces and Their Interactions with Aqueous Solutions and Microbial Organisms. *Chem. Rev.* **1999**, *99*, 77–174.
- (16) Von Rudorff, G. F.; Jakobsen, R.; Rosso, K. M.; Blumberger, J. Fast Interconversion of Hydrogen Bonding at the Hematite (001)-Liquid Water Interface. *J. Phys. Chem. Lett.* **2016**, *7*, 1155–1160.
- (17) Stoerzinger, K. A.; Hong, W. T.; Crumlin, E. J.; Bluhm, H.; Biegalski, M. D.; Shao-Horn, Y. Water Reactivity on the LaCoO<sub>3</sub> (001) Surface: An Ambient Pressure X-Ray Photoelectron Spectroscopy Study. *J. Phys. Chem. C* **2014**, *118*, 19733–19741.
- (18) Stoerzinger, K. A.; Hong, W. T.; Crumlin, E. J.; Bluhm, H.; Shao-Horn, Y. Insights into Electrochemical Reactions from Ambient Pressure Photoelectron Spectroscopy. *Acc. Chem. Res.* **2015**, *48*, 2976–2983.
- (19) Comes, R.; Chambers, S. Interface Structure, Band Alignment, and Built-In Potentials at LaFeO<sub>3</sub>/n-SrTiO<sub>3</sub> Heterojunctions. *Phys. Rev. Lett.* **2016**, *117*, 226802.
- (20) Nakamura, K.; Mashiko, H.; Yoshimatsu, K.; Ohtomo, A. Impact of Built-in Potential across LaFeO<sub>3</sub>/SrTiO<sub>3</sub> Heterojunctions on Photocatalytic Activity. *Appl. Phys. Lett.* **2016**, *108*, 211605.
- (21) Nakamura, M.; Kagawa, F.; Tanigaki, T.; Park, H. S.; Matsuda, T.; Shindo, D.; Tokura,

- 1  
2  
3 Y.; Kawasaki, M. Spontaneous Polarization and Bulk Photovoltaic Effect Driven by Polar  
4 Discontinuity in LaFeO<sub>3</sub>/SrTiO<sub>3</sub> Heterojunctions. *Phys. Rev. Lett.* **2016**, *116*, 156801.  
5  
6  
7  
8  
9 (22) Xu, P.; Han, W.; Rice, P. M.; Jeong, J.; Samant, M. G.; Mohseni, K.; Meyerheim, H. L.;  
10 Ostanin, S.; Maznichenko, I. V.; Mertig, I.; et al. Reversible Formation of 2D Electron Gas  
11 at the LaFeO<sub>3</sub>/SrTiO<sub>3</sub> Interface via Control of Oxygen Vacancies. *Adv. Mater.* **2017**,  
12 1604447.  
13  
14  
15  
16  
17  
18  
19 (23) Jacobs, R.; Booske, J.; Morgan, D. Understanding and Controlling the Work Function of  
20 Perovskite Oxides Using Density Functional Theory. *Adv. Funct. Mater.* **2016**, *26*, 5471–  
21 5482.  
22  
23  
24  
25  
26  
27 (24) Makowski, M. J.; Galhenage, R. P.; Langford, J.; Hemminger, J. C. Liquid-Jet X-Ray  
28 Photoelectron Spectra of TiO<sub>2</sub> Nanoparticles in an Aqueous Electrolyte Solution. *J. Phys.*  
29 *Chem. Lett.* **2016**, *7*, 1732–1735.  
30  
31  
32  
33  
34  
35 (25) Starr, D. E.; Liu, Z.; Hävecker, M.; Knop-Gericke, A.; Bluhm, H. Investigation of  
36 Solid/vapor Interfaces Using Ambient Pressure X-Ray Photoelectron Spectroscopy. *Chem.*  
37 *Soc. Rev.* **2013**, *42*, 5833–5857.  
38  
39  
40  
41  
42  
43 (26) Crumlin, E. J.; Bluhm, H.; Liu, Z. In Situ Investigation of Electrochemical Devices Using  
44 Ambient Pressure Photoelectron Spectroscopy. *J. Electron Spectros. Relat. Phenomena*  
45 **2013**, *190*, 84–92.  
46  
47  
48  
49  
50  
51 (27) Lichterman, M. F.; Hu, S.; Richter, M. H.; Crumlin, E.; Axnanda, S.; Favaro, M.; Drisdell,  
52 W. S.; Hussain, Z.; Mayer, T.; Brunshwig, B. S.; et al. Direct Observation of the  
53 Energetics at a Semiconductor/Liquid Junction by Operando X-Ray Photoelectron  
54  
55  
56  
57  
58  
59  
60

- 1  
2  
3 Spectroscopy. *Energy Environ. Sci.* **2015**, *8*, 2409–2416.
- 4  
5  
6  
7 (28) Axnanda, S.; Scheele, M.; Crumlin, E.; Mao, B. H.; Chang, R.; Rani, S.; Faiz, M.; Wang,  
8 S. D.; Alivisatos, A. P.; Liu, Z. Direct Work Function Measurement by Gas Phase  
9 Photoelectron Spectroscopy and Its Application on PbS Nanoparticles. *Nano Lett.* **2013**,  
10 *13*, 6176–6182.
- 11  
12  
13  
14  
15  
16  
17 (29) Gonzalez-Elipe, A. R.; Espinos, J. P.; Fernandez, A.; Munuera, G. XPS Study of the  
18 Surface Carbonation/hydroxylation State of Metal Oxides. *Appl. Surf. Sci.* **1990**, *45*, 103–  
19 108.
- 20  
21  
22  
23  
24  
25 (30) Merino, N. A.; Barbero, B. P.; Eloy, P.; Cadús, L. E.  $\text{La}_{1-x}\text{Ca}_x\text{CoO}_3$  Perovskite-Type  
26 Oxides: Identification of the Surface Oxygen Species by XPS. *Appl. Surf. Sci.* **2006**, *253*,  
27 1489–1493.
- 28  
29  
30  
31  
32  
33 (31) Flynn, B. T.; Zhang, K. H. L.; Shutthanandan, V.; Varga, T.; Colby, R. J.; Oleksak, R. P.;  
34 Manandhar, S.; Engelhard, M. H.; Chambers, S. A.; Henderson, M. A.; et al. Growth and  
35 Surface Modification of  $\text{LaFeO}_3$  Thin Films Induced by Reductive Annealing. *Appl. Surf.*  
36 *Sci.* **2015**, *330*, 309–315.
- 37  
38  
39  
40  
41  
42  
43 (32) Becerra-Toledo, A. E.; Enterkin, J. A.; Kienzle, D. M.; Marks, L. D. Water Adsorption on  
44  $\text{SrTiO}_3(001)$ : II. Water, Water, Everywhere. *Surf. Sci.* **2012**, *606*, 791–802.
- 45  
46  
47  
48  
49 (33) Mefford, J. T.; Hardin, W. G.; Dai, S.; Johnston, K. P.; Stevenson, K. J. Anion Charge  
50 Storage through Oxygen Intercalation in  $\text{LaMnO}_3$  Perovskite Pseudocapacitor Electrodes.  
51 *Nat. Mater.* **2014**, *13*, 726–732.
- 52  
53  
54  
55  
56  
57 (34) Geneste, G.; Morillo, J.; Finocchi, F. Adsorption and Diffusion of Mg, O, and  $\text{O}_2$  on the  
58  
59  
60

- 1  
2  
3 MgO(001) Flat Surface. *J. Chem. Phys.* **2005**, *122*, 174707.
- 4  
5  
6  
7 (35) Worayingyong, A.; Kangvansura, P.; Ausadasuk, S.; Praserttham, P. The Effect of  
8 Preparation: Pechini and Schiff Base Methods, on Adsorbed Oxygen of LaCoO<sub>3</sub>  
9 Perovskite Oxidation Catalysts. *Colloids Surfaces A Physicochem. Eng. Asp.* **2008**, *315*,  
10 217–225.
- 11  
12  
13  
14  
15  
16  
17 (36) Kaliaguine, S.; Van Neste, A.; Szabo, V.; Gallot, J. E.; Bassir, M.; Muzychuk, R.  
18 Perovskite-Type Oxides Synthesized by Reactive Grinding. Part I. Preparation and  
19 Characterization. *Appl. Catal. A Gen.* **2001**, *209*, 345–358.
- 20  
21  
22  
23  
24  
25 (37) Newberg, J. T.; Starr, D. E.; Yamamoto, S.; Kaya, S.; Kendelewicz, T.; Mysak, E. R.;  
26 Porsgaard, S.; Salmeron, M. B.; Brown, G. E.; Nilsson, A.; et al. Formation of Hydroxyl  
27 and Water Layers on MgO Films Studied with Ambient Pressure XPS. *Surf. Sci.* **2011**,  
28 *605*, 89–94.
- 29  
30  
31  
32  
33  
34  
35 (38) Corberán, V. C.; Tejuca, L. G.; Bell, A. T. Surface Reactivity of Reduced LaFeO<sub>3</sub> as  
36 Studied by TPD and IR Spectroscopies of CO, CO<sub>2</sub> and H<sub>2</sub>. *J. Mater. Sci.* **1989**, *24*, 4437–  
37 4442.
- 38  
39  
40  
41  
42  
43 (39) Kendelewicz, T.; Kaya, S.; Newberg, J. T.; Bluhm, H.; Mulakaluri, N.; Moritz, W.;  
44 Scheffler, M.; Nilsson, A.; Pentcheva, R.; Brown, G. E. X-Ray Photoemission and  
45 Density Functional Theory Study of the Interaction of Water Vapor with the Fe<sub>3</sub>O<sub>4</sub> (001)  
46 Surface at Near-Ambient Conditions. *J. Phys. Chem. C* **2013**, *117*, 2719–2733.
- 47  
48  
49  
50  
51  
52  
53 (40) Yamamoto, S.; Kendelewicz, O. T.; Newberg, J. T.; Ketteler, G.; Starr, D. E.; Mysak, E.  
54 R.; Andersson, K. J.; Ogasawara, H.; Bluhm, H.; Salmeron, M.; et al. Water Adsorption  
55  
56  
57  
58  
59  
60

- 1  
2  
3 on  $\alpha$ -Fe<sub>2</sub>O<sub>3</sub> ( 0001 ) at near Ambient Conditions. *J. Phys. Chem. C* **2010**, *114*, 2256–2266.  
4  
5  
6  
7 (41) Feng, Z. A.; Balaji Gopal, C.; Ye, X.; Guan, Z.; Jeong, B.; Crumlin, E.; Chueh, W. C.  
8  
9 Origin of Overpotential-Dependent Surface Dipole at CeO<sub>2-x</sub>/Gas Interface During  
10  
11 Electrochemical Oxygen Insertion Reactions. *Chem. Mater.* **2016**, *28*, 6233–6242.  
12  
13  
14 (42) Sunding, M. F.; Hadidi, K.; Diplas, S.; Løvvik, O. M.; Norby, T. E.; Gunnæs, A. E. XPS  
15  
16 Characterisation of in Situ Treated Lanthanum Oxide and Hydroxide Using Tailored  
17  
18 Charge Referencing and Peak Fitting Procedures. *J. Electron Spectros. Relat. Phenomena*  
19  
20 **2011**, *184*, 399–409.  
21  
22  
23  
24 (43) Comes, R. B.; Xu, P.; Jalan, B.; Chambers, S. A. Band Alignment of Epitaxial SrTiO<sub>3</sub>  
25  
26 Thin Films with (LaAlO<sub>3</sub>)<sub>0.3</sub>-(Sr<sub>2</sub>AlTaO<sub>6</sub>)<sub>0.7</sub> (001). *Appl. Phys. Lett.* **2015**, *107*, 131601.  
27  
28  
29  
30 (44) Chambers, S. A.; Droubay, T. C.; Capan, C.; Sun, G. Y. Unintentional F Doping of  
31  
32 SrTiO<sub>3</sub>(001) Etched in HF Acid-Structure and Electronic Properties. *Surf. Sci.* **2012**, *606*,  
33  
34 554–558.  
35  
36  
37  
38 (45) Grass, M. E.; Karlsson, P. G.; Aksoy, F.; Lundqvist, M.; Wannberg, B.; Mun, B. S.;  
39  
40 Hussain, Z.; Liu, Z. New Ambient Pressure Photoemission Endstation at Advanced Light  
41  
42 Source Beamline 9.3.2. *Rev. Sci. Instrum.* **2010**, *81*, 53106.  
43  
44  
45  
46  
47  
48  
49  
50  
51  
52  
53  
54  
55  
56  
57  
58  
59  
60

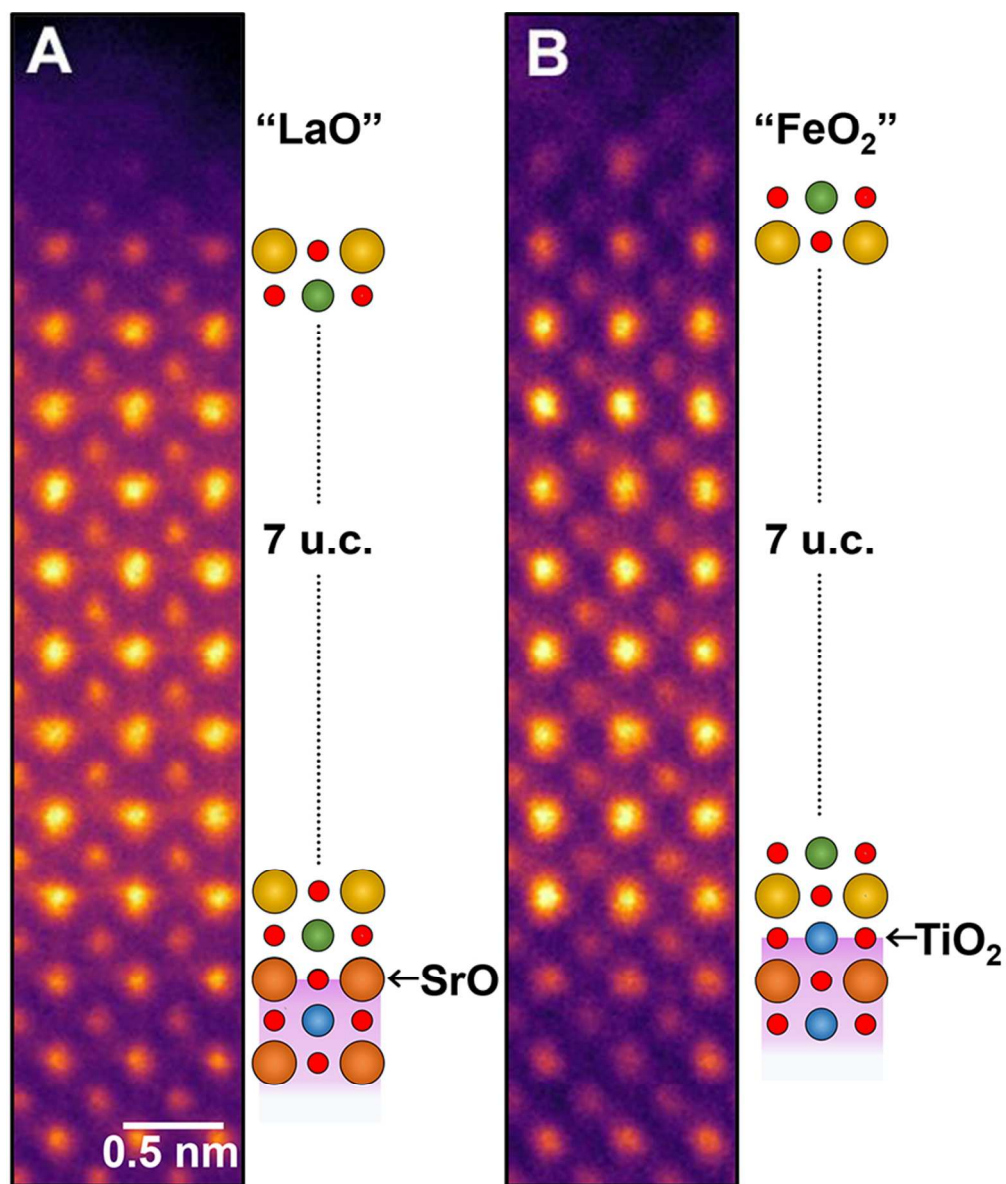


Figure 1. Colored cross-sectional STEM-HAADF images and schematics of the 9 unit cell (u.c.)  $\text{LaFeO}_3/\text{Nb}:\text{SrTiO}_3$  films fabricated by oxygen assisted MBE.  $\text{LaO-LFO}$  was grown on a  $\text{SrO}$ -terminated substrate (A), and  $\text{FeO}_2\text{-LFO}$  was grown on a  $\text{TiO}_2$ -terminated one (B). Surface terminations were confirmed by angle resolved XPS (Table S1).<sup>19</sup>

Figure 1

76x89mm (300 x 300 DPI)

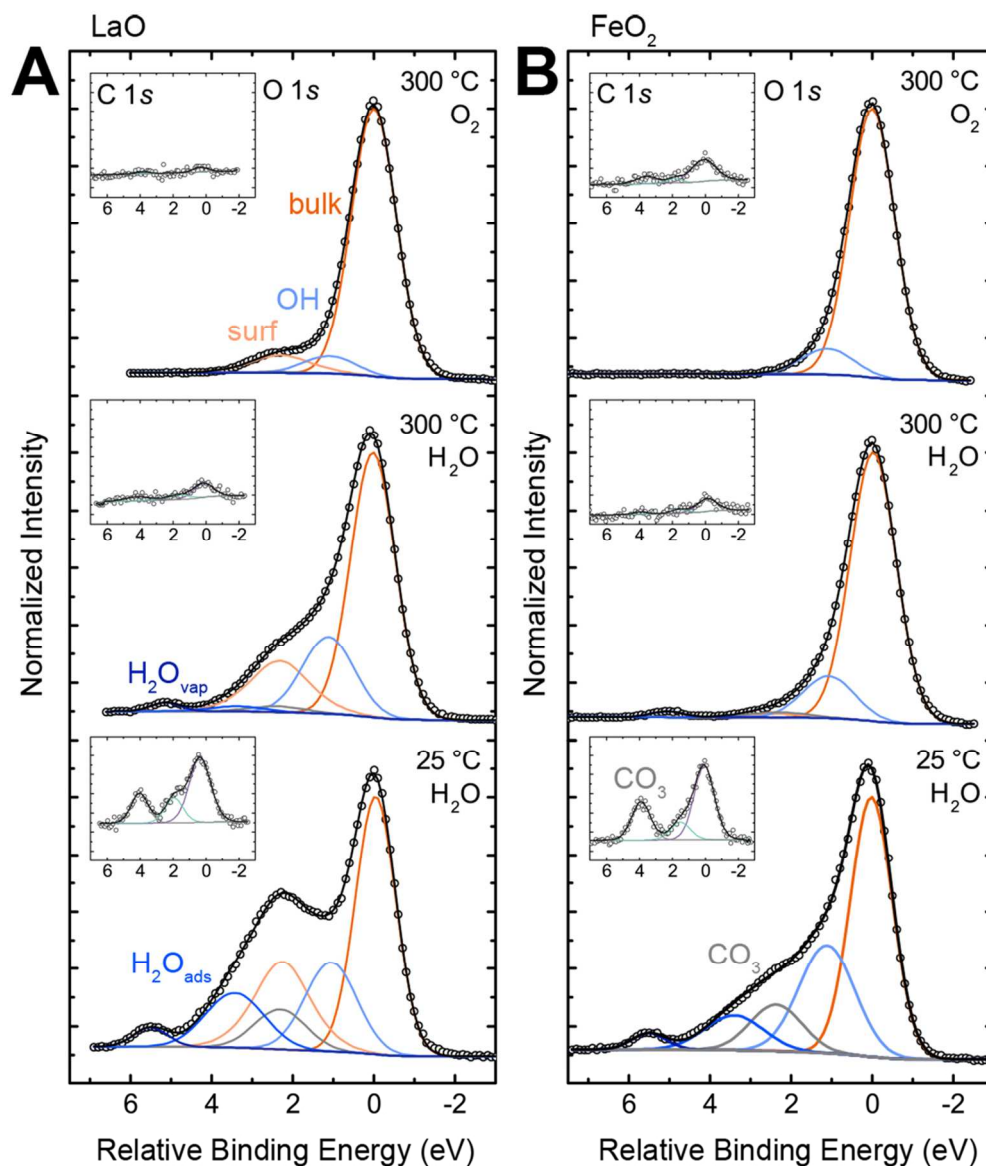


Figure 2. O 1s spectra and C 1s spectra (inset) for (A) LaO-LFO and (B) FeO<sub>2</sub>-LFO at 300 °C in 100 mTorr O<sub>2</sub> (top), 300 °C in 100 mTorr H<sub>2</sub>O (middle) and 25 °C in 100 mTorr H<sub>2</sub>O (bottom). Raw data are shown as points with fitted components and envelope (black) as lines. O 1s components correspond to the bulk oxide (orange), hydroxide (light blue), carbonate (gray), surface (peach), adsorbed water (medium blue), and gas phase water (dark blue). C 1s components correspond to carbonate (gray), adventitious carbon (purple), and an intermediate carbon oxidation (teal). The binding energy scale is shown relative to the bulk oxide (O 1s) and adventitious carbon (C 1s) to better illustrate relative offsets of species in fitting.

Figure 2

107x125mm (300 x 300 DPI)



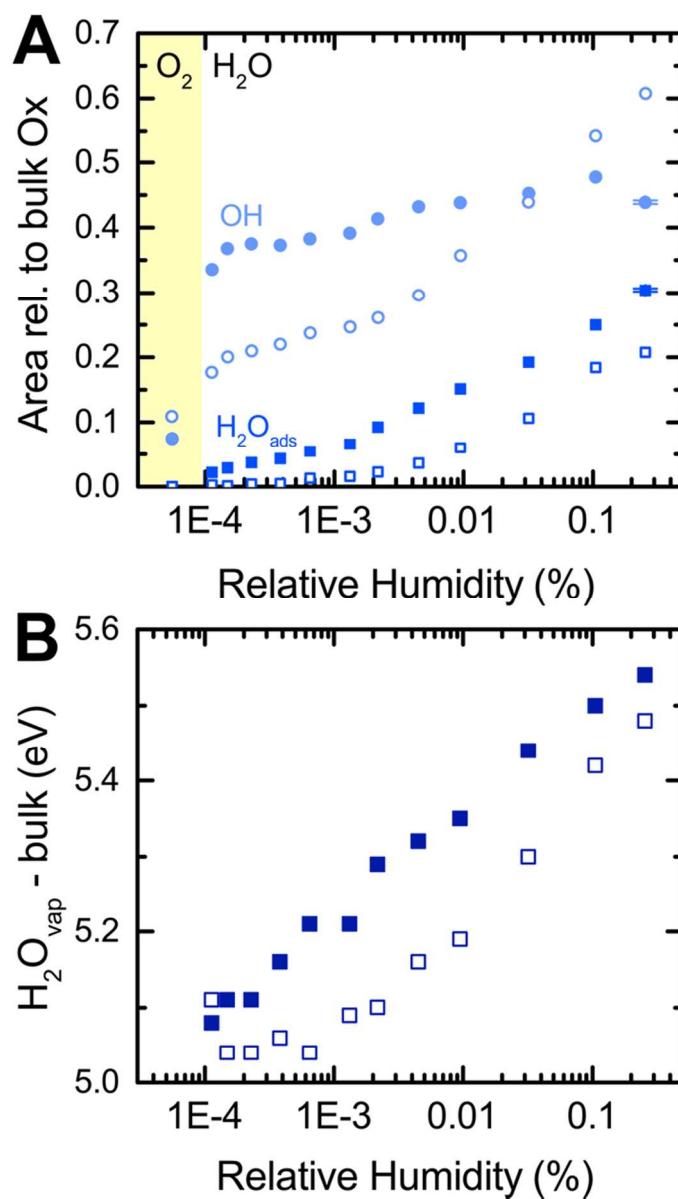


Figure 3. (A) Area of the OH (light blue, circles) and H<sub>2</sub>O<sub>ads</sub> (medium blue, squares) normalized to that of the bulk oxide as a function of RH probed by changing temperature in a 100 mTorr H<sub>2</sub>O isobar. Dry conditions (300 °C in 100 mTorr O<sub>2</sub>) are indicated with a yellow bar. LaO-LFO (solid) is more reactive toward water compared to FeO<sub>2</sub>-LFO (open). (B) Location of the gas-phase H<sub>2</sub>O<sub>vap</sub> peak relative to the bulk oxygen peak for LaO-LFO (solid) and FeO<sub>2</sub>-LFO (open) as a function of RH. The increase in binding energy corresponds to a decrease in sample work function, or formation of a surface dipole aiding photoelectron removal.

Figure 3

60x107mm (300 x 300 DPI)

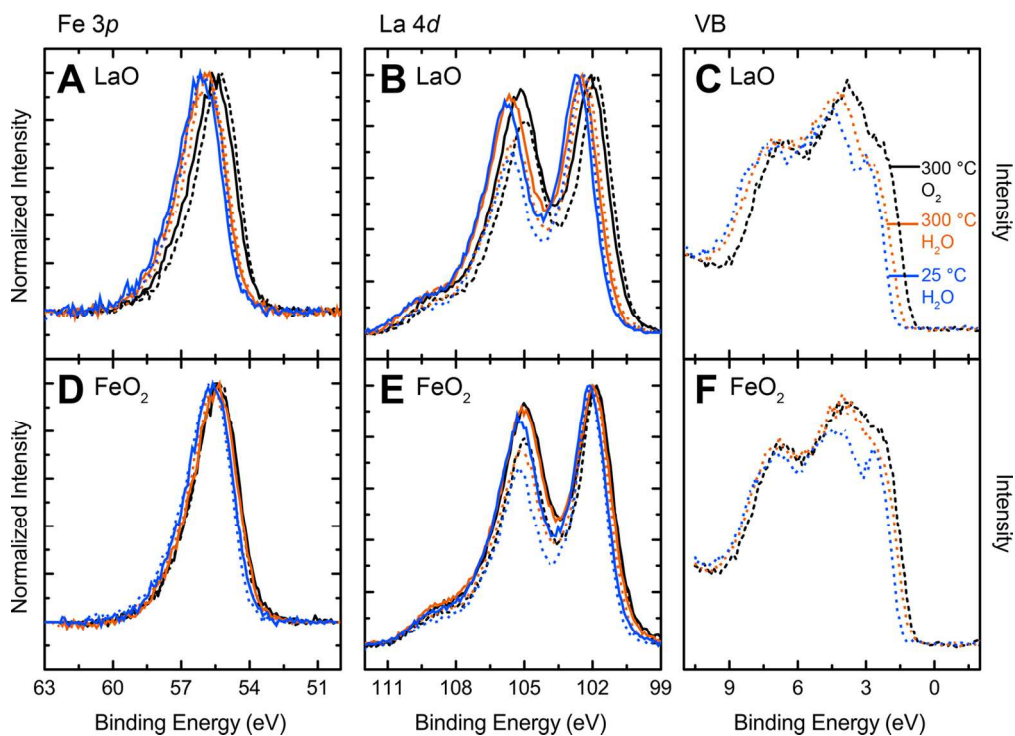


Figure 4. Noted Fe 3p, La 4d core levels and valence band (VB) for (A-C) LaO-LFO and (D-F) FeO<sub>2</sub>-LFO. Solid lines are for 690 eV incident photon energy with a larger information depth than dashed lines for 350 eV. Conditions are 300 °C in 100 mTorr O<sub>2</sub> (black), 300 °C in 100 mTorr H<sub>2</sub>O (orange) and 25 °C in 100 mTorr H<sub>2</sub>O (blue). The shift to higher binding energies with increasing RH corresponds to downward band bending, and is greater for LaO-LFO.

Figure 4.

139x102mm (300 x 300 DPI)